

# Adsorption of H<sub>2</sub>O, CO<sub>2</sub> and Xe on Soft Surfaces

Ori Stein and Micha Asscher\*

Department of Physical Chemistry and the Farkas Center for Light-Induced Processes,  
The Hebrew University of Jerusalem, Israel

Received: October 12, 2007; In Final Form: January 10, 2008

The interactions of water, carbon dioxide, and Xe with octadecanethiol (C<sub>18</sub>H<sub>37</sub>SH, ODT) self-assembled monolayers (SAMs) were studied under ultrahigh vacuum conditions employing temperature-programmed desorption and optical diffraction measurements. The ODT layer was grown on a 1 nm thick gold film deposited over a Ru(001) single-crystal substrate. The gases used in this report differ in their lateral interactions while adsorbed on ODT-SAM being either repulsive (Xe) or attractive (H<sub>2</sub>O, CO<sub>2</sub>). The activation energies for desorption of the first layer from ODT are  $E_a = 3.6 \pm 0.9$ ,  $4.1 \pm 0.5$ , and  $8.5 \pm 0.9$  kcal/mol for Xe, CO<sub>2</sub>, and H<sub>2</sub>O, respectively. Sticking probabilities of the three gases on the soft ODT surface are  $S_0 = 0.7 \pm 0.1$ ,  $0.8 \pm 0.1$ , and  $0.95 \pm 0.05$  for xenon, CO<sub>2</sub>, and water, respectively, derived from the respective adsorption curves. Optical diffraction studies from multilayer coverage grating of Xe on ODT-SAM have demonstrated that sublimation is a thermodynamically more favorable process over diffusion and wetting. The significantly lower binding energy of the first layers of H<sub>2</sub>O and CO<sub>2</sub> adsorbed on the soft surface of ODT compared to that on clean metals and oxides, reflects generally weak (CO<sub>2</sub>) and hydrophobic (H<sub>2</sub>O) interactions that are important for understanding the behavior of these molecules on interfaces that are found in biological systems.

## 1. Introduction

The interaction and structure of adsorbates on top of “soft” interfaces prepared from self-assembled monolayers (SAMs) is of interest in many fields of science and technology.<sup>1–3</sup> These SAMs form densely packed, smooth yet relatively flexible monolayers when compared to solid surfaces of metals and oxides.

The interaction of water and CO<sub>2</sub> on top of SAMs may serve as a model for gaining molecular level understanding of the chemistry of these small molecules with biologically relevant surfaces such as membranes. In addition to water and carbon dioxide, Xe atoms were recently demonstrated also as potential biologically relevant biosensor in medical MRI applications.<sup>4</sup> An earlier study has discussed the interaction and binding of D<sub>2</sub>O on top of SAM layers composed of hydrophobic CH<sub>3</sub>-terminated and hydrophilic OH-terminated SAMs.<sup>5,6</sup> This study, based on temperature-programmed desorption (TPD) and IR measurements, have focused on the effect of the different substrates on the binding and interaction of D<sub>2</sub>O with organic surfaces.

Accurate determination of the binding energy of water molecules at the first and thicker layers on hydrophobic surfaces is important for fundamental insight into phenomena such as diffusion on the surface of membranes and membrane crossing. It is surprising, therefore, to realize that very few experimental studies exist that provide data at the level of precision that can be obtained under well-defined, model ultrahigh vacuum (UHV) conditions. In our study here, we have limited ourselves to the hydrophobic, CH<sub>3</sub>-terminated SAM, which is more relevant as a model for biologically important surfaces. We have focused on the role of small molecules of different chemical character, which are also important for living, biological functions.

Growing stable organic SAMs typically requires a well-defined gold substrate, if the chemical link is via a thiol end group. The growth of gold on ruthenium (our substrate in this study) has been extensively studied over the past two decades. The motivation has often been to understand basic metal on metal growth modes, structural, and fundamental catalysis.<sup>8–10</sup> The growth mode of gold is sensitive to the ruthenium substrate structure and temperature.<sup>10</sup>

The introduction of scanning tunneling microscopy (STM) revealed interesting new observations related to the growth mechanism and structure of thin metal films, e.g., Au, Ag, and Cu,<sup>11–13</sup> on top of ruthenium. Upon deposition at room temperature, gold atoms form 2D islands that are often structurally complex, originating from diffusion limited aggregation (DLA) growth mechanism. Annealing these structures to 650 K completely changes their morphology and causes reconstruction of the film. This is even more pronounced at annealing temperature above 1000 K.<sup>11</sup>

The interaction and structure of water on solid surfaces has been studied in great detail from the experimental and theoretical points of view.<sup>14–25</sup> Water interacting with clean Ru(001) (an important calibration system for this work) is a system that has attracted particular interest and has generated contradicting results.<sup>14–16</sup> Ab initio calculations have suggested that water partially dissociates on top of Ru(001) surface.<sup>17</sup> Low-energy electron diffraction (LEED) and TPD studies following the theoretical hypothesis have reported results in favor<sup>18</sup> but also in contrast<sup>19</sup> to the partial dissociation idea. In contrast to ruthenium, it is well-established that on top of gold surfaces water do not dissociate. Only a single work has so far discussed the interaction of water on top of hydrocarbon-terminated SAM surfaces;<sup>5,6</sup> see below.

The growth procedure and structure of SAMs on gold and many other surfaces has been described in detail in ref 26 and can be considered as an introduction to the formation of “soft”

\* To whom correspondence should be addressed. E-mail: asscher@fh.huji.ac.il.

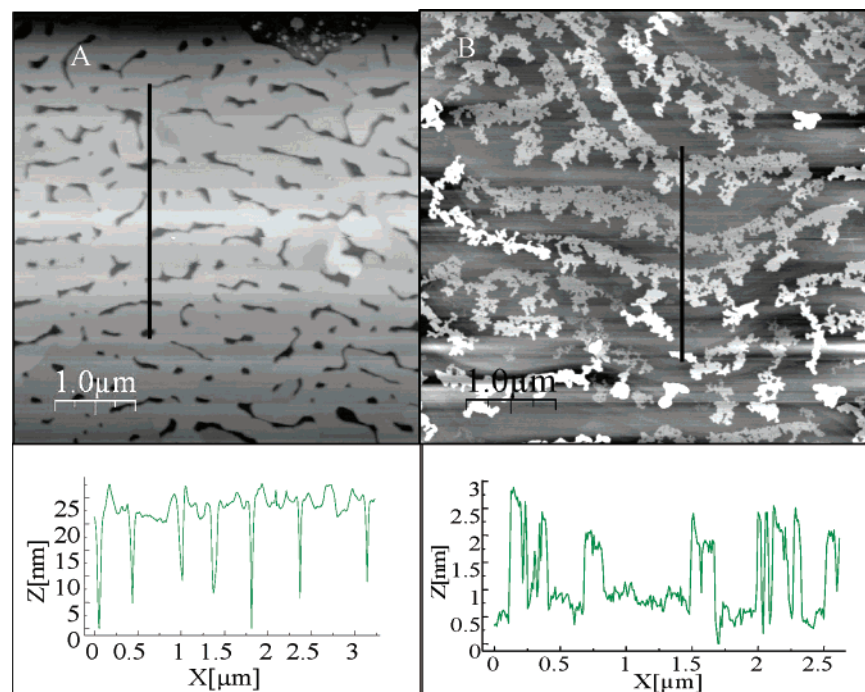


**Figure 1.** (A) AFM image of 20 nm thick Au film on Ru(001). Line scan along the solid line reveals average troughs depth of  $\sim 20$  nm. (B) 2 nm thick Au on Ru(001) deposited at 650 K. 3D islands of gold grow on top of a wetting film below.

surfaces in general.<sup>26</sup> Crystal structure of an alkanethiolate SAM was reported to be commensurate with the gold surface and having  $(\sqrt{3} \times \sqrt{3}) R30^\circ$  unit cell with the sulfur atoms at the end of the chain at a hollow site on the gold surface.<sup>27</sup> Top adsorption of thiolate chain on the same surface accompanied by reconstruction of the top gold layer was also claimed.<sup>28,29</sup> The interaction of  $D_2O$  on top of mixed SAMs consisting of  $CH_3$ -,  $OH$ -, and  $COOCH_3$ -terminating groups<sup>5,6</sup> was studied by employing TPD and IR absorption reflection spectroscopy (IRAS) in UHV. The authors suggested that  $D_2O$  adsorbed on a  $CH_3$ -terminating SAM undergoes a phase transformation from amorphous to crystalline when heated from 82 to 140 K. Upon cooling, the transformation was not reversible, indicating meta stability of the amorphous phase. Phase transformation did not occur in the  $OH$ -terminating SAM until 150 K, the onset of desorption. TPD analysis of their data has led these authors to conclude that water forms clusters of different shapes on  $CH_3$ - and  $OH$ -terminated SAM, being spherical, and 3D on the  $CH_3$ -terminated, hydrophobic SAM and were closer to flat 2D clusters on the  $OH$  terminated, hydrophilic SAM. This fact leads to a different number of possible binding sites, theoretically supported by Monte Carlo simulations.<sup>30</sup> An activation energy for desorption of  $D_2O$  from a  $CH_3$ -terminated SAM of 9.8 kcal/mol was estimated (with a pre-exponent of  $\nu = 10^{13} \text{ s}^{-1}$  and first-order kinetics), indicating a typical hydrogen-bonded system, as expected in 3D water clusters.

In this work, we present a TPD-based study of  $H_2O$ ,  $CO_2$ , and Xe from an octadecanethiol ( $C_{18}H_{37}SH$ , ODT) SAM. The nature of interactions of these gas species with SAMs varies considerably. The influence of the hydrophobic ( $CH_3$ -terminated) SAM and the significantly different interaction of these gases on the bare Ru(001) surface will be discussed.

This paper provides, therefore, a new insight into the interaction of important and abundant small molecules (water and carbon dioxide) with soft, organic surfaces and thus defining their behavior on top of surfaces that can provide a model for biologically important interfaces.

## 2. Experimental

The experiments described in this work have been performed in a UHV chamber with a base pressure of  $5 \times 10^{-10}$  mbar. The chamber was equipped with a  $Ne^+$  sputter gun for sample cleaning. A quadrupole mass spectrometer (QMS, VG SX-200) was used for TPD experiments, its ionizer enclosed in a glass shroud having a 5-mm aperture at its end. The QMS was mounted on a retractable bellow that enabled aperture approach to 1 mm from the sample. This chamber was also equipped with a gold evaporator, a tungsten filament wrapped around a gold wire (5 mm long, 1 mm diameter 99.999% pure). The evaporator was also enclosed within a glass shroud in order to fine-tune its position with respect to the sample. Evaporation rates were calibrated using quartz microbalance, and the total dosage of gold was in the range of 1–20 nm in terms of gold film thickness. Finally, LEED was also used in order to characterize the long-range structure of the surface. Xe (99.9999% pure),  $CO_2$  (99.95% pure), and triple distilled water (TDW) were introduced by backfilling the UHV chamber via high precision leak valves up to a pressure of  $5 \times 10^{-8}$  mbar. This procedure ensures homogeneous surface coverage at multilayer coverage, at the expense of operating at higher background pressures.<sup>31</sup> The TDW were cleaned from air content via three freeze–pump–thaw cycles.

The Ru(001) sample, 1 mm thick, 8 mm in diameter, was used throughout, spot welded to tantalum wires attached via copper rods to a closed cycle helium cryostat (APD) cooling down to 25 K. Sample temperature was monitored using W26%Re–W5%Re thermocouple wires, providing the necessary input for a computer routine that resistively heat and control the sample temperature in the range of 25–1600 K.

After standard cleaning procedure, which included three cycles of  $Ne^+$  ion bombardment at energies of 1200, 900, and 700 eV and annealing the sample to 1620 K, gold atoms were deposited on the Ru surface. The resulting gold surface was subsequently characterized using LEED (hexagonal pattern

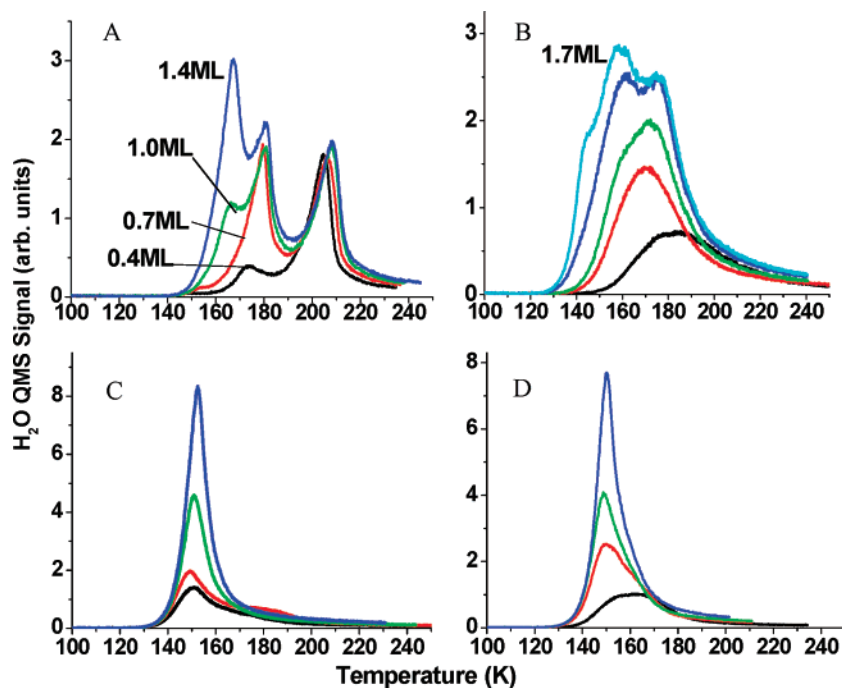


**Figure 2.** H<sub>2</sub>O TPD in the coverage range (the same color code for all four frames) of 0.4–1.7 ML from: (A) clean ruthenium, (B) 0.8 Å thick gold deposited on ruthenium, (C) 1.6 Å thick gold, (D) 2.5 Å thick gold. The TPD runs were performed at 1 K/s.

suggests mostly Au(111) orientation) and smooth ex situ in air AFM images (DI 3100, TESP tip, working in tapping mode).

The Ru/Au sample was then removed from the vacuum chamber and placed in a 1 mM ODT solution in ethanol for 24 h in order to grow the SAM. Upon removal from the solution, the sample was dipped ten times in pure ethanol and then dried under helium purge in air. The resulting SAM surface was subsequently imaged by AFM in order to verify its perfect compact and smooth top surface.

To perform thermal stability measurements (diffusion and desorption upon sample heating) of atomic or molecular layers on the ODT-SAM surface, a *p*-polarized Nd:YAG pulsed laser working at the fundamental wave length was used ( $\lambda = 1.064 \mu\text{m}$ , 10-ns pulse duration). Absorbed laser power by the ruthenium metal substrate was kept lower than  $2.5 \text{ MW/cm}^2$  to avoid damage to the SAM layer. The procedure has been as follows: A weakly bound gas material, such as Xe, is adsorbed on the surface. A single, split-laser pulse at a 1:1 intensity ratio recombines on the surface, in this case, at an angle of about  $\theta = \pm 6^\circ$  with respect to the surface normal. The absorbed laser generates a sinusoidal spatial temperature profile on the surface, which ablates part of the weakly bound material via laser-induced thermal desorption process. This process leaves behind stripes of adsorbed gas. In situ characterization of such patterns is possible by detecting optical linear diffraction from such coverage grating using He-Ne laser (cw, 5 mW,  $\lambda = 638.2 \text{ nm}$ ). By recording optical linear diffraction (first and second order) while performing TPD experiment, one can study the thermal stability of adsorbates.<sup>31</sup> When performing such experiments, one can observe whether there is multilayer diffusion (indicated by diffraction order intensity decay) of the patterned adsorbate before desorption onset. This is the common behavior of adsorbates on metal surfaces at sub-monolayer coverage.

### 3. Results and Discussion

**3.1. Gold Layer on Ru(001).** Numerous experimental studies in the past two decades have attempted to model and character-

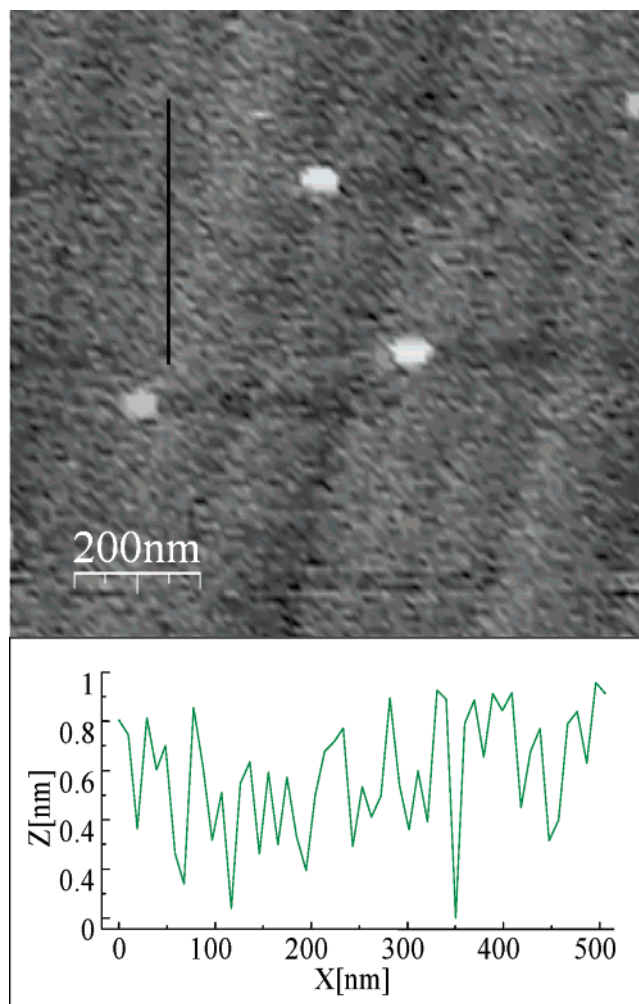


**Figure 3.**  $1 \times 1 \mu\text{m}$  AFM image of 1 nm thick gold on Ru(001) evaporated at 30 K, then annealed to 650 K for 1 min. The line scan reveals the level of surface corrugation.

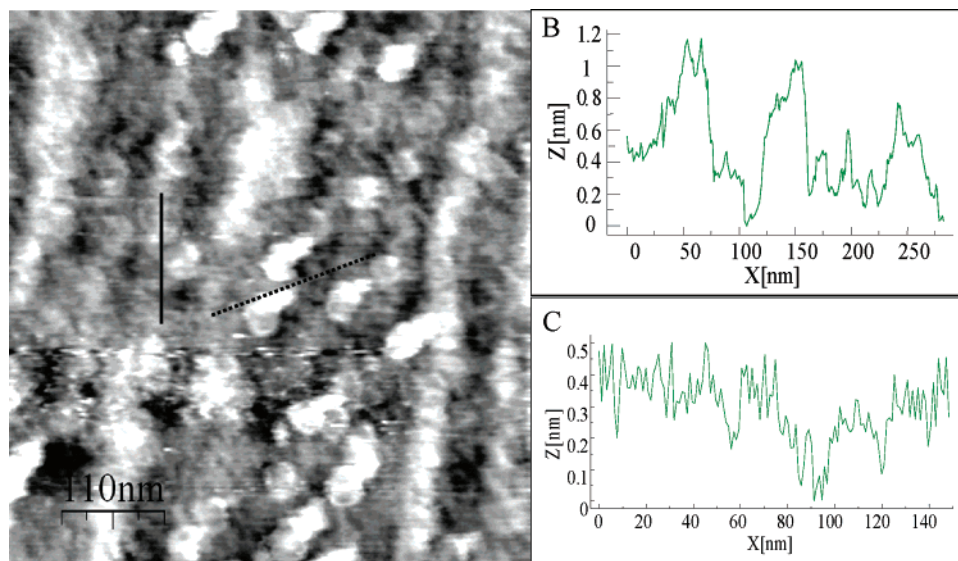


**Figure 4.** AFM image of ODT-SAM on top of a 1 nm thick gold film, with a scan size of  $550 \times 550$  nm. (B) Line scan along the dotted line, reflects imperfections within the ODT layer, up to  $8 \text{ \AA}$  high. Line scan (C, solid line) reveals a roughness level similar to the gold film underneath.

ize layer growth and reconstruction of gold on ruthenium both experimentally<sup>9–11</sup> and theoretically.<sup>32</sup> In our work, several parameters were changed in order to examine their influence on the quality of the resulting film of gold. The evaporation procedure has been modified by changing the gold dosage at different surface temperatures and under various sample annealing schemes. Figure 1A shows the result of AFM image obtained following deposition of 20 nm of gold on the Ru(001) surface held at 650 K. In this image, the 3D nature of the gold layer is apparent with large smooth patches containing elongated valleys,  $20 \pm 2$  nm deep. This depth measurement, supported by interpretation of the AFM phase image (not shown) has led us to believe that the initial 1–2 layers of gold completely wet the ruthenium surface. At further dosage, the gold layer began to grow 3D, as often is the case in heteroatomic metal on metal growth. A similar procedure, but reducing the gold dosage to 2 nm, results in ramified 3D islands on top of smooth terraces as depicted in Figure 1B, consistent with previous studies.<sup>10</sup> Prior to, in between, and after completion of the 2 nm thick layer of gold, LEED images were taken, which demonstrated sharp, intense peaks from the clean Ru(001) in the characteristic hexagonal pattern and diffuse peaks from the gold-covered ruthenium. This suggests the predominance of the (111) plane, indicating diminished long-range order with respect to Ru(001). The image in Figure 1B was obtained after annealing of the surface to 1100 K.

Water TPD has been used as a complementary characterization tool to AFM in order to verify completion of gold coverage on top of the ruthenium surface. AFM measurements are sensitive to height of features but not at all to their chemical composition, making it difficult to verify the homogeneity of the gold layer.

Interaction and bonding of water on Ru(001) has been extensively studied in recent years.<sup>16–19</sup> Water has a unique TPD spectrum from Ru(001), consisting of three well-separated peaks that can be attributed to multilayer of amorphous solid water (ASW) at 155–160 K, molecules directly interacting with the clean ruthenium at  $\sim 180$  K and a unique, high-temperature peak at 210 K, the nature of which is still not fully understood. It seems, however, to be associated with water molecules interacting with nearby  $\text{OH}_{\text{ad}}$  or  $\text{O}_{\text{ad}}$ .<sup>17</sup> This peak is extremely sensitive to surface impurities, mostly adsorbed oxygen. The disappearance of that high-temperature peak and the major change in

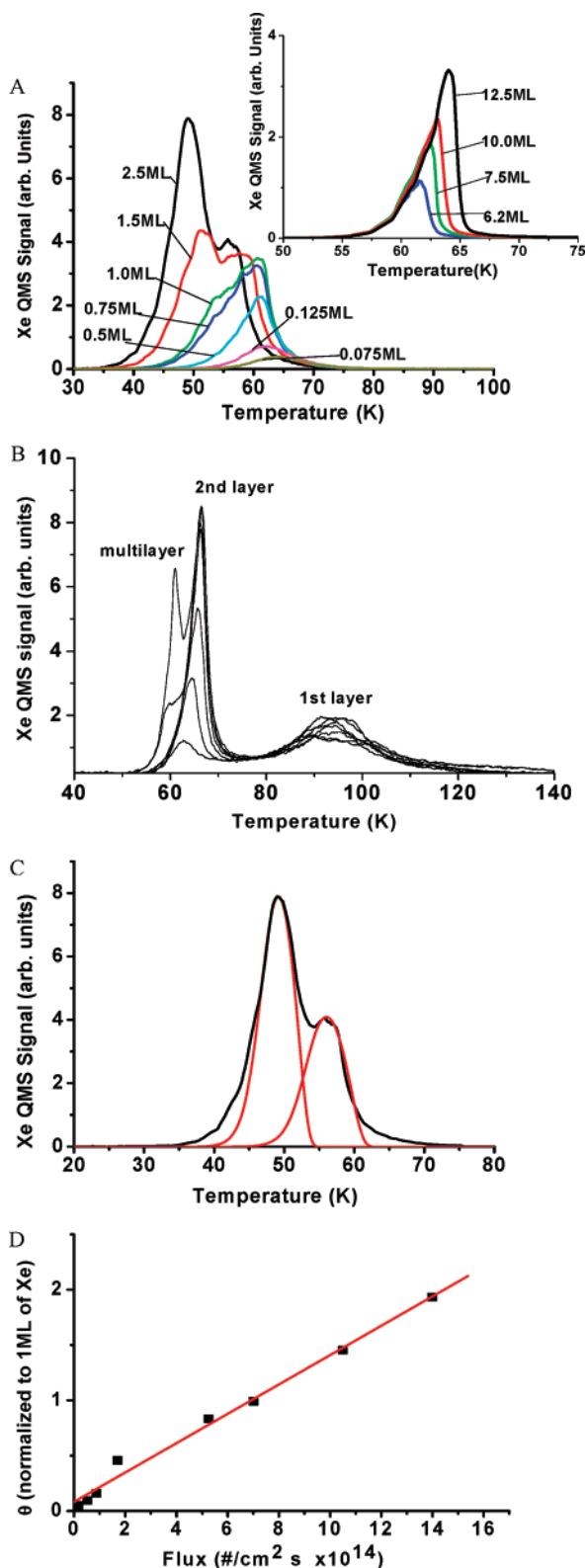
the TPD spectrum of water on Ru were examined while evaporating different amounts of gold. Furthermore, gold deposition on top of a cold (30 K) ruthenium substrate was chosen to avoid atom diffusion and aggregation at the deposition stage. The dosage of gold atoms has been determined by a quartz microbalance in units of angstroms. We have deposited two consecutive dosages of  $2.5 \text{ \AA}$  and compared this to a single dose of  $5 \text{ \AA}$ . These cycles were added up to a total gold dosage of  $10 \text{ \AA}$ . After each evaporation cycle, the sample was annealed to 650 K and was held at that temperature for 1 min. Prior to the annealing process, TPD spectra of water at different exposures were taken as a titration for remaining patches of clean, exposed Ru(001) surfaces, shown in Figure 2. From a typical  $\text{H}_2\text{O}/\text{Ru}(001)$  TPD pattern, a gradual transition to a TPD of  $\text{H}_2\text{O}$  desorbing from inert substrates is observed upon gold deposition. It is evident that already after evaporation of  $1.6 \text{ \AA}$  of gold the Ru surface is nearly fully covered by gold, except for a minor signature of bare ruthenium shown as a hump in the TPD spectra at 180 K (Figure 2C);  $2.5 \text{ \AA}$  of gold completely masks the bare Ru(001) surface.

Figure 3 is an AFM image of 1 nm of gold deposited on top of a cold (30 K) Ru surface (as mentioned, evaporation took place in stages described above). One can see that 1 nm of gold, directly deposited over a cold surface and subsequently annealed to 650 K for 1 min is enough to produce a rather smooth surface (see Figure 1B for comparison). This growth mode became our sample preparation scheme throughout. On top of these relatively smooth gold surfaces we have subsequently studied SAM growth and interaction of gases on top of it.

### 3.2. Interaction of Gases with “Soft” Organic Interface.

**3.2.1. Xe on ODT-SAM.** After producing a 1-nm smooth layer of gold on top of Ru(001), the sample was removed from the UHV chamber and then placed in 1 mM ODT ( $\text{C}_{18}\text{H}_{37}\text{SH}$ ) in ethanol for 24 h. The resulting ODT-SAM was characterized by AFM, as shown in Figure 4. Differences in texture of the layer compared to clean gold are clearly seen and possibly reflect some level of imperfection in the growth of the SAM film.<sup>33</sup>

The strength of interaction of Xe,  $\text{H}_2\text{O}$ , and  $\text{CO}_2$  was subsequently examined via TPD experiments. These gases differ in their typical interaction with metallic surfaces. Xe and  $\text{CO}_2$  often repel their neighboring species while adsorbed on metallic surfaces.  $\text{H}_2\text{O}$  molecules, in contrast, always attract their neighbors due to hydrogen bonding. Xe TPD spectra for various



**Figure 5.** Xe TPD (recorded at 66 amu, the doubly ionized (Xe) QMS signal) from (A)  $C_{18}SH/Au/Ru$  surface, Xe coverage range of 0.075–2.5 ML. Inset: multilayer Xe TPD, at a coverage range of 5–12.5 ML. (B) Xe TPD from clean Ru(001), 1.2–2 ML. Heating rate was 1 K/s. (C) Double peak analysis (see text) of 2 ML Xe desorbing from ODT-SAM, heating rate was 1 K/s. Solid line: experimental data. Red solid line: line shape analysis based on Redhead equation, fitted to the first and second desorption peaks, based on first-order desorption kinetics. (D) Adsorption curve of Xe. Flux normalized to ionization gauge sensitivity factor. Solid line is a linear fit to the experimental data. Coverage ( $\theta$ ) is normalized to 1 ML of Xe. The slope which represents the sticking coefficient is:  $S_0(Xe, ODT) = 0.7 \pm 0.1$ .

coverages (exposures) are presented in Figure 5. The TPD profile consists of two peaks at low coverages up to the completion of two layers. The strength of interaction Xe-ODT-SAM was derived from a Redhead line-shape analysis with activation energy for desorption of the first layer  $E_a^1(Xe, ODT) = 3.6 \pm 0.7$  kcal/mol, assuming first-order kinetics and pre-exponent factor of  $1 \times 10^{13} s^{-1}$ . For comparison, activation energy for desorption of the first layer from clean Ru(001) surface is almost twice larger,  $E_a^1(Xe, Ru) = 6.1 \pm 0.1$  kcal/mol<sup>33,34</sup> demonstrated in Figure 5B. The covalent C–H bonds in the surface-exposed  $CH_3$  groups at the surface of organic SAM weakens the interaction and thus the physisorption energy within the Xe-ODT-SAM system. This is in contrast to Xe physisorption on metal surfaces, where enhanced polarizability of the metals enables stronger overall Xe–metal bonding.

To calculate the activation energy for desorption of the second layer, TPD line-shape analysis was performed (based on a Redhead procedure), after separating the double peaked spectrum into their two component spectra. This procedure result in activation energy for desorption of  $E_a^2(Xe, ODT) = 2.9 \pm 0.7$  for the second layer. This is 1 kcal/mol lower compared with the value obtained for desorption of the second layer from clean ruthenium. Evidently, surface influence is apparent even at coverages  $> 1$  ML. As the coverage increases, the desorption peak temperature converges to the known value for multilayers desorbing from metallic surfaces at  $63 \pm 3$  K.<sup>31</sup> The sticking probability ( $S_0$ ) of Xe on the ODT-SAM surface was derived from the slope of the adsorption curve as presented in Figure 5D, being  $S_0(Xe, ODT) = 0.7 \pm 0.1$ . This is somewhat smaller than the value obtained on metals, which is consistent with the weaker interaction of Xe on the ODT surface.

Next, we have addressed the issue of wetting/diffusion vs desorption in the Xe multilayer.<sup>31,35</sup> We have employed the experimental setup described in detail in ref 31. Briefly, a Xe coverage grating has been created on top of the ODT-SAM surface using a laser ablation procedure as described in the experimental section and in refs 36 and 37. After adsorbing an amount of Xe equal to 100 ML, a split 2.5 MW/cm<sup>2</sup> laser pulse from a Nd:YAG laser impinges on the surface, forming a thermally stable periodic density modulation referred to as a coverage grating. The sample was then turned 90° to face the QMS. While facing the QMS and heating the sample, detection of the first- or second-order optical diffraction peaks took place (using He–Ne 5-mW laser) while simultaneously recording the QMS signal of desorbing Xe atoms. The results are presented in Figure 6.

The derivatives of the first- and second-order optical diffraction spectra as a function of temperature during sample temperature ramp do not change in intensity all the way to the desorption onset at about 50 K. We conclude that desorption is the thermodynamically favorable process that xenon undergoes rather than diffusion and wetting. If diffusion were to take place instead of desorption, one would have seen decay of the first-order linear diffraction signal prior to the onset of desorption. In particular, it should be seen in the case of the more sensitive second-order diffraction signal. Similar results were obtained over clean Ru(001) as reported in ref 31.

**3.2.2.  $CO_2$  on ODT-SAM.** The interaction of  $CO_2$  with the ODT-SAM surface is slightly stronger than that of Xe and is attractive among neighbor-adsorbed  $CO_2$  molecules. TPD spectra of  $CO_2$  from ODT-SAM are presented in Figure 7A. It is possible to see the buildup of the second layer at exposures above 0.5 L (possibly due to 3D islands forming before completion of the first layer). Moreover, as coverage increases,

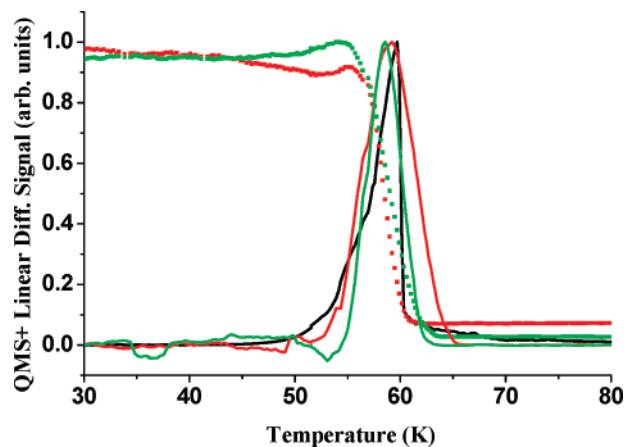


**Figure 6.** Simultaneous recording of TPD (100 ML Xe) and linear first and second order optical (He-Ne laser) diffraction decay, at a heating rate of 1 K/s. Solid black line, TPD of 100 ML Xe; green and red squares, normalized first- and second-order linear diffraction signals, respectively; green and red solid curves, derivatives of the first- and second-order linear diffraction signals, respectively.

the peak desorption temperature shifts upward to 78 K at 10 ML. Inspection of the peak desorption temperature of  $\text{CO}_2$  from ODT to that of  $\text{CO}_2$  from various other substrates, metals and oxides reveals that  $\text{CO}_2$  desorbs from the organic surface at a significantly lower temperature. For example, from Ru,  $\text{CO}_2$  desorbs at 100 K;<sup>38</sup> from oxygen-covered Ag(110),  $\text{CO}_2$  desorbs molecularly at 130 K and has another high-temperature peak at 480 K due to decomposition of surface carbonate ( $\text{CO}_3$ ) to  $\text{CO}_2$  and  $\text{O}_{\text{ad}}$ .<sup>39</sup> By assumption of a pre-exponent factor of  $1 \times 10^{13} \text{ s}^{-1}$  and first-order desorption, the activation energy of the first layer has the value of  $E_{\text{a}}^1(\text{CO}_2 \text{ ODT}) = 4.1 \pm 0.5 \text{ kcal/mol}$ . By curve fitting the second layer TPD peak at a coverage of 6.6 ML, as in Figure 5C, a value of  $E_{\text{a}}^2(\text{CO}_2, \text{ ODT}) = 4.4 \pm 0.6 \text{ kcal/mol}$  was obtained (see Figure 7). The gradual shift of desorption peaks to higher temperature with increasing coverage can be attributed to growing  $\text{CO}_2$  islands, already at a sub-monolayer coverage.<sup>40,41</sup> Island formation requires fast  $\text{CO}_2$  diffusion on the ODT-SAM surface already at surface temperatures as low as 50 K. The activation energy for desorption reported here is significantly lower compared with desorption from metal surfaces as reported, e.g., in ref 42. The low activation energy for desorption and the indication of low-temperature island formation (desorption temperature increases with cluster size) emphasizes the weaker interaction of  $\text{CH}_3$ -terminated ODT-SAM with  $\text{CO}_2$  adsorbates compared with the interaction between neighboring  $\text{CO}_2$  molecules.

With an increase in coverage from 6 to 10 ML, one can clearly see a 3–4° shift in the desorption onset. This shift may be attributed to coalescence of 3D  $\text{CO}_2$  islands thus causing an increase in binding energy among neighbor clusters. The phenomenon seems to be characteristic for all adsorbates that possess an attractive interaction between neighbors (Similar results were obtained with water on ODT-SAM, as described below).

The adsorption curve of  $\text{CO}_2$  could be obtained based on a comparison with the uptake of water from clean Ru(001) for which the total number of molecules in 1 ML is accurately known (not shown), taking into account the QMS sensitivity factor for these two molecules. The sticking probability derived this way was  $S_0(\text{CO}_2, \text{ ODT}) = 0.8 \pm 0.1$ . This is a high value relative to the sticking coefficient of  $\text{CO}_2$  on metallic surfaces like copper, derived from molecular beam studies,  $S_0(\text{CO}_2, \text{ Cu}) = 0.43 \pm 0.03$ .<sup>42</sup> This may originate from the softness and large

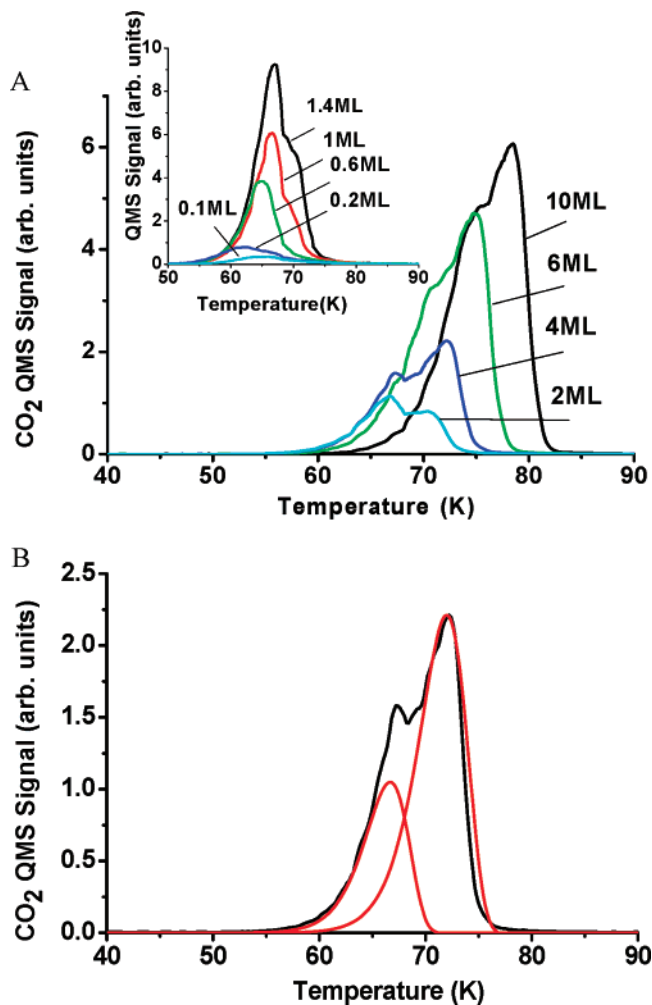


**Figure 7.** (A) TPD of  $\text{CO}_2$  from ODT-SAM at coverages of 2–10 ML. Inset:  $\text{CO}_2$  TPD of 0.1–1.4 ML. Heating rate is 1 K/s. (B) Double-peak curve fitting to TPD spectrum of 6.6 ML  $\text{CO}_2$ , see text.

number of degrees of freedom of the ODT-SAM surface, effectively absorbing a fraction of the incident kinetic energy of  $\text{CO}_2$ , thus leading to its sticking and adsorption on the surface. On the other hand, the weak interaction between  $\text{CO}_2$ - and  $\text{CH}_3$ -terminated ODT-SAM should present a very low barrier for diffusion of  $\text{CO}_2$ , thus leading to island formation already at low temperature of 50 K.

Measuring the binding energy of  $\text{CO}_2$  to organic ODT-SAM presents the first information of its kind. It may prove important for external  $\text{CO}_2$  skin and internal lung surface interactions with  $\text{CO}_2$ , where removal of the intact  $\text{CO}_2$  and its inert behavior are crucial.<sup>43</sup>

**3.2.3.  $\text{H}_2\text{O}$  on ODT-SAM.** The binding of water molecules to  $\text{CH}_3$ -terminated ODT-SAM has been studied as an example of inter-adsorbate attractive interaction systems on a hydrophobic substrate. Water TPD spectra at different initial coverage are presented in Figure 8. The onset of desorption is at 120 K. For comparison, the onset of desorption at sub-monolayer coverage from metallic surfaces such as gold and ruthenium are 127 and 180 K (Figure 2), respectively. This low desorption temperature demonstrates the hydrophobic nature of the system composed of water and the ODT-SAM. An interesting feature can be seen in the inset of Figure 8: with an increase in the coverage from 1 to 2 ML one may observe a sudden temperature increase of 3–4° at the desorption onset. Normally, for zero-order reactions, as in the case of water, the leading edge of TPD spectra overlap up to the peak temperature, regardless of

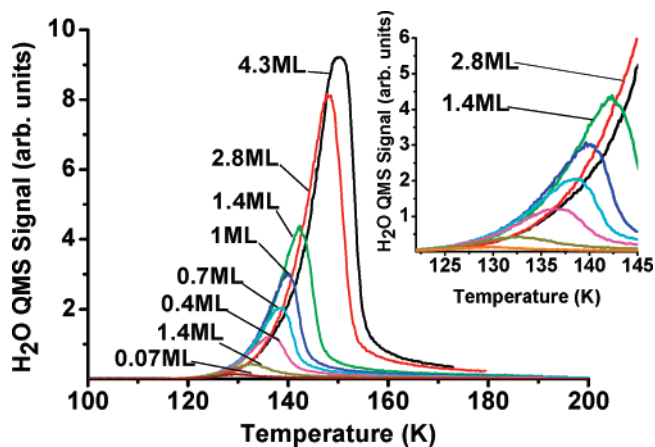


**Figure 8.** TPD of H<sub>2</sub>O from ODT-SAM at coverages of 0.07–4.3 ML. The spectra show a single, gradually growing peak with no sign of saturation. An interesting feature is a sudden shift of 3 K at the desorption onset, between the curves at 1.4 and 2.8 ML, see text. Inset: Magnification of the temperature range reflecting the onset for desorption.

coverage, with a gradual upward shift of the desorption rate maximum. Here we see a slight shift, indicating the influence of hydrogen bonds among the water molecules as their density increases, forming islands at sub-monolayer coverage. The increase in overall binding (shift of the desorption to higher temperature) as clusters start to form at the second layer, can be rationalized by the extra hydrogen-bonding that can occur for molecules at the second layer. Comparison with the TPD spectrum of water from a Au(111) surface as presented in Figure 2 and ref 25 reveals that the spectra obtained from the ODT-SAM are rather similar to those recorded from smooth gold. The obvious difference is in this unique upward temperature shift observed only in the ODT system and recorded also with CO<sub>2</sub>, as mentioned in section 3.2.2 above. In their study of D<sub>2</sub>O desorption from CH<sub>3</sub>-terminated SAMs, the authors of ref 5 have not reported this kind of temperature shift, possibly due to the small difference in hydrogen bonding of D<sub>2</sub>O vs H<sub>2</sub>O. Comparison of the TPD spectra obtained when water molecules desorb from OH- and CH<sub>3</sub>-terminated SAMs<sup>5</sup> (as in our case) reveals broader spectra from hydrophobic SAMs, while IRAS data supported amorphous water to polycrystalline phase transformation. These authors concluded that since the CH<sub>3</sub>-terminated surface enables enhanced mobility of water molecules and cannot form hydrogen bonds with the surface, in contrast to the OH-terminated SAM, the phase transformation occurs continuously during sample heating. This enables desorption from different sites, contributing to broadening of the TPD spectra, thus preventing assignment of a unique desorption kinetic order.

A line shape analysis of the H<sub>2</sub>O desorption yields an activation energy for desorption of  $E_a^1(\text{H}_2\text{O}, \text{ODT}) = 8.5 \pm 0.9$  kcal/mol assuming zero-order kinetics with a pre-exponent factor of  $1 \times 10^{13} \text{ s}^{-1}$ . The sticking probability was extracted from adsorption curves with a value of  $S_0(\text{H}_2\text{O}, \text{ODT}) = 0.95 \pm 0.05$ . This is associated with fast diffusion and cluster formation of H<sub>2</sub>O on the SAM-covered surface already at sub-monolayer water coverage, as is typical also of clean metal surfaces.<sup>44</sup> The authors of ref 5 have reported a significantly lower sticking coefficient ( $S_0(\text{H}_2\text{O}, \text{SAM}) = 0.4$ ), but their experiments were performed at a surface temperature of 120 K, practically the desorption onset, which explains the significantly different values of  $S_0$  obtained in these two studies.

#### 4. Conclusions

We have studied the strength of interaction of several gas molecules (H<sub>2</sub>O, CO<sub>2</sub>) and atom (Xe) on top of ODT-SAM under UHV conditions. Prior to the self-assembly of the ODT monolayer, a smooth 1 nm thick film of gold was obtained by deposition on a 30 K Ru(001) single-crystal surface with subsequent annealing to 650 K. The morphology of the gold film was then characterized using AFM imaging. This Au/Ru(001) substrate was subsequently used for the growth of the ODT-SAM.

Activation energies for desorption of Xe, CO<sub>2</sub>, and water and their sticking probabilities were derived from the TPD data. In both Xe and CO<sub>2</sub>, the first layer desorption and multilayer could be distinguished as separate desorption peaks. Surprisingly, the strength of interaction of CO<sub>2</sub> with the ODT-SAM is significantly weaker than its interaction with metallic surfaces, decreasing the peak desorption temperature from 95 K ( $E_a^1(\text{CO}_2, \text{Ru}(001)) = 5.8$  kcal/mol) to 57 K ( $E_a^1(\text{CO}_2, \text{ODT}) = 4.1$  kcal/mol), at monolayer coverage. We conclude that the ODT-SAM molecular film prevents any chemisorption and charge transfer between the underlying metal surface and the adsorbed CO<sub>2</sub> molecules.<sup>30</sup> This information is predicted to be significant and important for molecular level quantitative understanding of the interaction of CO<sub>2</sub> with biological interfaces such as internal “soft” surfaces of lungs in living species.

Water, similar to CO<sub>2</sub>, exhibited a weaker interaction on hydrophobic ODT-SAM compared to a metal surface. Quantitative determination of H<sub>2</sub>O-organic SAM interaction is needed for basic understanding of most biological interfaces.

Finally, xenon interaction with the ODT-SAM gradually becomes weaker as coverage increases, a similar trend as observed on metals due to repulsion among neighboring adsorbed atoms. The monolayer activation energy for desorption was found to be almost half the activation energy for desorption of the monolayer xenon from ruthenium. This may be related to the lack of free electrons at the ODT-SAM surface. Similar to the behavior on metals, multilayer Xe sublimates and does not wet the ODT-SAM surface, as indicated by from coverage-grating optical diffraction studies.

**Acknowledgment.** This research was partially supported by a grant from the US–Israel Binational Science Foundation by the Israel Science Foundation and the German Israel Foundation. The Farkas Center is supported by the Bundesministerium für Forschung und Technologie and the Minerva Gesellschaft für die Forschung mbh.

#### References and Notes

- (1) Epple, M.; Bittner, A. M.; Kuhnke, K.; Kern, K.; Zheneq, W.-Q.; Tadjeddine, A. *Langmuir* **2002**, *18*, 773.
- (2) Tai, Y.; Shaporenko, A.; Noda, H.; Grunze, M.; Zharnikov, M. *Adv. Mater.* **2005**, *17*, 1745.
- (3) Park, S.; Keavney, D. J.; Falco, C. M. *J. Appl. Phys.* **2004**, *95*, 3037.
- (4) Hilty, C.; Lowery, T. J.; Wemmer, D. E.; Pines, A. *Angew. Chem., Int. Ed.* **2006**, *45*, 70.
- (5) Engquist, I.; Lundström, I.; Leidberg, B. *J. Phys. Chem.* **1995**, *99*, 12257.
- (6) Engquist, I.; Lundström, I.; Leidberg, B. *J. Phys. Chem.* **1995**, *99*, 14198.
- (7) Galvagno, S.; Schwank, J.; Parravano, G.; Garbassi, F.; Marzi, A.; Tauszik, G. R. *J. Catal.* **1981**, *69*, 283.
- (8) Bassi, I. W.; Garbassi, F.; Valic, G.; Marzi, A.; Tauszik, G. R. *J. Catal.* **1980**, *64*, 405.
- (9) Park, C. *Surf. Sci.* **1988**, *203*, 395.
- (10) Steltenpohl, A.; Memmel, N.; Taglauer, E.; Fauster, Th.; Onsgaard, J. *Surf. Sci.* **1997**, *382*, 300.

- (11) Hwang, R. Q.; Schröder, J.; Günther, C.; Behm, R. J. *Phys. Rev. Lett.* **1991**, *67*, 3279.
- (12) Pötschke, G. O.; Behm, R. J. *Phys. Rev. B* **1991**, *44*, 1442.
- (13) Parschau, M.; Schlatterbeck, D.; Christmann, K. *Surf. Sci.* **1997**, *376*, 133.
- (14) Doering, D. L.; Madey, T. E. *Surf. Sci.* **1982**, *123*, 305.
- (15) Henderson, M. A. *Surf. Sci. Rep.* **2002**, *46*, 1.
- (16) Scott Smith, R.; Huang, C.; Wong, E. K. L.; Kay, B. D. *Surf. Sci. Lett.* **1996**, *367*, L13.
- (17) Feibelman, P. J. *Science* **2002**, *295*, 99.
- (18) Weissenreider, J.; Mikkelsen, A.; Andersen, J. N.; Held, G. *Phys. Rev. Lett.* **2004**, *93*, 1961021.
- (19) Denzler, D. N.; Hess, Ch.; Dudek, R.; Wagner, S.; Frischkorn, Ch.; Wolf, M.; Ertl, G. *Chem. Phys. Lett.* **2003**, *376*, 618.
- (20) Stevenson, K. P.; Kimmel, G. A.; Dohnálek, Z.; Scott Smith, R.; Kay, B. D. *Science* **1999**, *283*, 1505.
- (21) Held, G.; Menzel, D. *Surf. Sci.* **1994**, *316*, 92.
- (22) Zhang, Q.; Buch, V. *J. Chem. Phys.* **1990**, *92*, 5004.
- (23) Speedy, R. J.; Debenedetti, P. G.; Scott Smith, R.; Huang, C.; Kay, B. D. *J. Chem. Phys.* **1996**, *105*, 240.
- (24) Kimmel, G. A.; Petrik, N. G.; Dohnálek, Z.; Kay, B. D. *J. Chem. Phys.* **2006**, *125*, 0447131.
- (25) Kay, B. D.; Lykke, K. R.; Randall, J.; Ward, S. J. *J. Chem. Phys.* **1989**, *91* (8), 5120.
- (26) Ulman, A. *Chem. Rev.* **1996**, *96*, 1533.
- (27) Alves, C. A.; Smith, E. L.; Porter, M. D. *J. Am. Chem. Soc.* **1992**, *114*, 1222.
- (28) Barth, J. V.; Brune, H.; Ertl, G.; Behm, R. J. *Phys. Rev. B* **1990**, *42*, 9307.
- (29) Roper, M. G.; Skegg, M. P.; Fisher, C. J.; Lee, J. J.; Dhanak, V. R.; Woodruff, D. P.; Jones, R. G. *Chem. Phys. Lett.* **2004**, *389*, 87.
- (30) Hautmann, J.; Klein, M. L. *Phys. Rev. Lett.* **1991**, *67*, 1763.
- (31) Kerner, G.; Stein, O.; Lilach, Y.; Asscher, M. *Phys. Rev. B* **2005**, *71*, 2054141.
- (32) Kuhn, M.; Rodriguez, J. A.; Hrbek, J.; Bzowski, A.; Sham, T. K. *Surf. Sci. Lett.* **1995**, *341*, L1011.
- (33) Maksymvych, P.; Sorescu, D. C.; Yates, J. T., Jr. *Phys. Rev. Lett.* **2006**, *97*, 1461031.
- (34) Widdra, W.; Trischberger, P.; Freiss, W.; Menzel, D. *Phys. Rev. B* **1998**, *57*, 4111.
- (35) Stein, O.; Asscher, M. Manuscript in preparation.
- (36) Kerner, G.; Asscher, M. *Nano Lett.* **2004**, *4* (8), 1433.
- (37) Kerner, G.; Asscher, M. *Surf. Sci.* **2004**, *557*, 5.
- (38) Berger, R.; Lilach, Y.; Ayoub, Y.; Asscher, M. *Isr. J. Chem.* **2005**, *45*, 97.
- (39) Freund, H. J.; Roberts, M. W. *Surf. Sci. Rep.* **1996**, *25*, 225.
- (40) Elliot, G. S.; Wu, K. J.; Kevan, S. D. *Chem. Phys. Lett.* **1990**, *175* (4), 371.
- (41) Ernst, K. H.; Schlatterbeck, D.; Christmann, K. *Phys. Chem. Chem. Phys.* **1999**, *1*, 4105.
- (42) Funk, S.; Hokkanen, B.; Wang, J.; Burghaus, U.; Bozzolo, G.; Garcés, J. E. *Surf. Sci.* **2006**, *600*, 583.
- (43) Bramble, D. M.; Carrier, D. R. *Science* **1983**, *291*, 251.
- (44) Lilach, Y.; Buch, V.; Asscher, M. *J. Chem. Phys.* **2003**, *119* (22), 11899.